A Time-Sharing Current-Fed ZCS High Frequency Inverter-Based Resonant DC-DC Converter with Si-IGBT/SiC-SBD Hybrid Module for Inductive Power Transfer Applications

Mishima, Tomokazu

(Citation)
IEEE Journal of Emerging and Selected Topics in Power Electronics,8(1):506-516

(Issue Date)
2019-07-10

(Resource Type)
journal article

(Version)
Accepted Manuscript

(URL)
https://hdl.handle.net/20.500.14094/90006177

This article has been accepted for publication in a future issue of this journal, but has not been fully edited. Content may change prior to final publication. Citation information: DOI 10.1109/JESTPE.2019.2927723, IEEE Journal of Emerging and Selected Topics in Power Electronics

A Time-Sharing Current-Fed ZCS High Frequency Inverter-Based Resonant DC-DC Converter with Si-IGBT / SiC-SBD Hybrid Module for Inductive Power Transfer Applications

Tomokazu Mishima, *Senior Member, IEEE,*

***Abstract*—This paper presents a time-sharing frequency doubler principle-based current-fed zero current soft-switching (ZCS) high frequency resonant (HF-R) inverter based dc-dc converter for inductive power transfer (IPT) systems featuring a Silicon (Si) and Silicon Carbide (SiC) hybrid power module. The newly-proposed resonant dc-dc converter is suitable for producing a higher frequency resonant current with switching power loss reduction by the effect of a high speed punch trough Si-Insulated gate bipolar transistor (IGBT) and low-forward voltage SiC-Schottky Barrier Diode (SBD). In order to continuously regulate the output power, resonant current phasor control based on phase shift modulation (PSM) is newly applied. The performances of the newly-proposed IPT resonant power converter are demonstrated by experiment, after which the feasibility of the circuit topology and control method is discussed from a practical point of view.**

Keywords*—high frequency-resonant (HF-R) inverter, inductive power transfer (IPT), phase shift modulation (PSM), series/parallel (SP) compensation, Si-IGBT / SiC-SBD hybrid power module, time-sharing principle, zero current soft-switching (ZCS).

I. Introduction

The latest developments of wide band gap (WBG) power devices such as Silicon Carbide (SiC) and Gallium Nitride (GaN) transistors revive the post-generation power converter topologies for the emerging resonant converter applications with higher switching frequency and high efficiency due to cutting-edge electron devices and package technologies[1][2]. As one of the emerging power electronics applications, IPT systems have drawn much attention in the wide variety areas of industrial and automotive electric power supplies such as battery chargers in Automated Guided Vehicle (AVG) and Electric Vehicles[3][4]. A typical power converter architecture of IPT system is depicted in Fig.1.

SiC-MOSFET and GaN-HEMT provide a high-frequency switching which is beneficial especially for several-hundred kHz operation. However, the low reliability and ruggedness as well as high cost still remain obstacles for adoption of the WBG power devices into the practical power conversion systems[5]-[7]. Silicon insulated gate bipolar transistor (Si-IGBT) has also been progressing greatly, featuring the low saturation voltage and excellent short circuit capability due to a new trench gate structure, chip and package technologies. Hence, the Si-IGBT still contributes as a primary selection of switching power device for the resonant power converter applications. In particular for IPT systems of the automotive applications, the standard frequency is $85\,\mathrm{kHz}$, hence adoption of a high-speed type Si-IGBT is more practical and cost effective than the WBG power devices in terms of voltage and current ratings as well as the gate driving technologies.

In contrast to the WBG-based active switches, SiC-Schottky Barrier Diode (SBD) technology has been disseminated into the wide areas of switch-mode power converter applications by now, featuring the low forward voltage, excellent thermal characteristics and reverse recovery-less operation[8]. Therefore, the hybrid power module of a high-speed Si-IGBT and SiC-SBD is a future promising power device for automotive and industrial power converters as well as home appliances and consumer electronics. This hybrid power module also exhibits more reliability and cost-effectiveness in dealing with the gate driving circuit and EMI noise mitigation as compared to all SiC power module[9][10].

Reduction of switching power losses and elimination of switching noises are also critical requirements for the switch-mode power converters, especially with high frequency switching. Zero current soft switching (ZCS) is suitable for the MOS-gate controlled Si-IGBT because a voltage and current overlapping interval due to a tail current can be avoided by the effect of moderate di/dt rate at turn-on and turn-off transitions. A current-fed high frequency-resonant (HF-R) inverter that is featured by the ride-through capability and a full-wave low-distortion, i.e. unity load-power-factor resonant current is quite useful for constituting the dc-dc converter stage in IPT systems[11]-[17]. This type of HF-R inverter operates with a full-wave resonant current under the condition of the voltage and current in-phase or the current-phase leading (capacitive load impedance), accordingly ZCS technique is quite effective for the current-fed HF-R inverter with Si-IGBT.

Having said that, extension of switching frequency has been a technical challenge for the IGBT-based power converters. As a first step of developments pertaining to the technical challenge, the time-sharing current-fed HF-R Thyristor inverter was proposed way back in [18], featuring minimization of switching losses owing to low switching frequency and ZCS operations. The switching frequency which is limited under several kHz in the externally commutated power device can be increased by adopting the self commutated Si-IGBT. The HF-R inverter with the self-commutated IGBT has been originally presented by the author of this paper for induction

T. Mishima, the corresponding author is with the Department of Marine Engineering, Graduate School of Maritime Science, Kobe University, Hyogo, Japan.(e-mail: mishima@maritime.kobe-u.ac.jp).

This article has been accepted for publication in a future issue of this journal, but has not been fully edited. Content may change prior to final publication. Citation information: DOI 10.1109/JESTPE.2019.2927723, IEEE Journal of Emerging and Selected Topics in Power Electronics

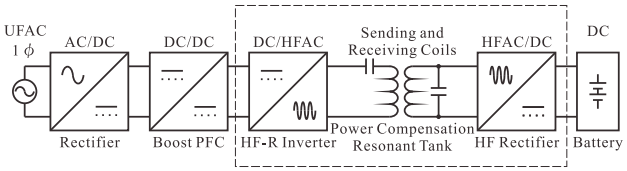

Fig. 1. Power conversion process of battery charger IPT system.

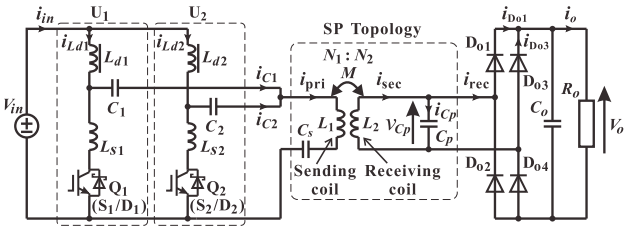

Fig. 2. A proposed resonant DC-DC converter using a time-sharing two-phase class-E ZCS inverter.

heating applications[19]. In the proposed HF-R inverter, a high frequency current, e.g. 100 kHz, which is twice or multiple times as much as the switching frequency, can be produced effectively even with middle speed-range (20 kHz–50 kHz) Si-IGBT which features a good balance between voltage and current ratings suitable for kW-class power processing.

A technical challenge of the time sharing inverter is how to reduce the power consumption of the anti-parallel diode which conducts during the negative half-cycle of resonant current through the active switches. In order to apply the time sharing inverter into the IPT system under the conditions of minimization of switching losses and reduction of the conduction losses, a Si-IGBT / SiC-SBD-embedded resonant dc-dc power converter with a time-sharing current-fed ZCS HF-R inverter is proposed in this paper.

The rest of this paper is organized as follows. The circuit topology and operating principle are explained with the outstanding features in Section II. The theory of output power control with phase shift modulation (PSM) for the time sharing inverter is described in Section III together with the resonant and switching frequency design guideline which is based on the sending and receiving coils modeling. Furthermore, the experimental verifications of the proposed circuit and the effectiveness of Si-IGBT / SiC-SBD module are demonstrated in Section IV, after which the summary is described in Section V.

II. Proposed Circuit Topology and Operations

A. Topology and Operating Mode Transitions

A schematic diagram of the proposed IPT power converter is illustrated in Fig.2. The operating waveforms, mode transitions and equivalent circuits during the switching one cycle are depicted in Figs.3 and 4, respectively.

The proposed HF-R inverter consists of the two-phase Class-E ZCS inverters U_1 and U_2 which share a sending coil in series with the power factor tuned capacitor C_s. The two-phase Class-E ZCS HF-R inverters are composed of DCLs L_{d1}, L_{d2} ($L_{d1} = L_{d2}$), ZCS-assisted inductors L_{s1}, L_{s2} ($L_s =$

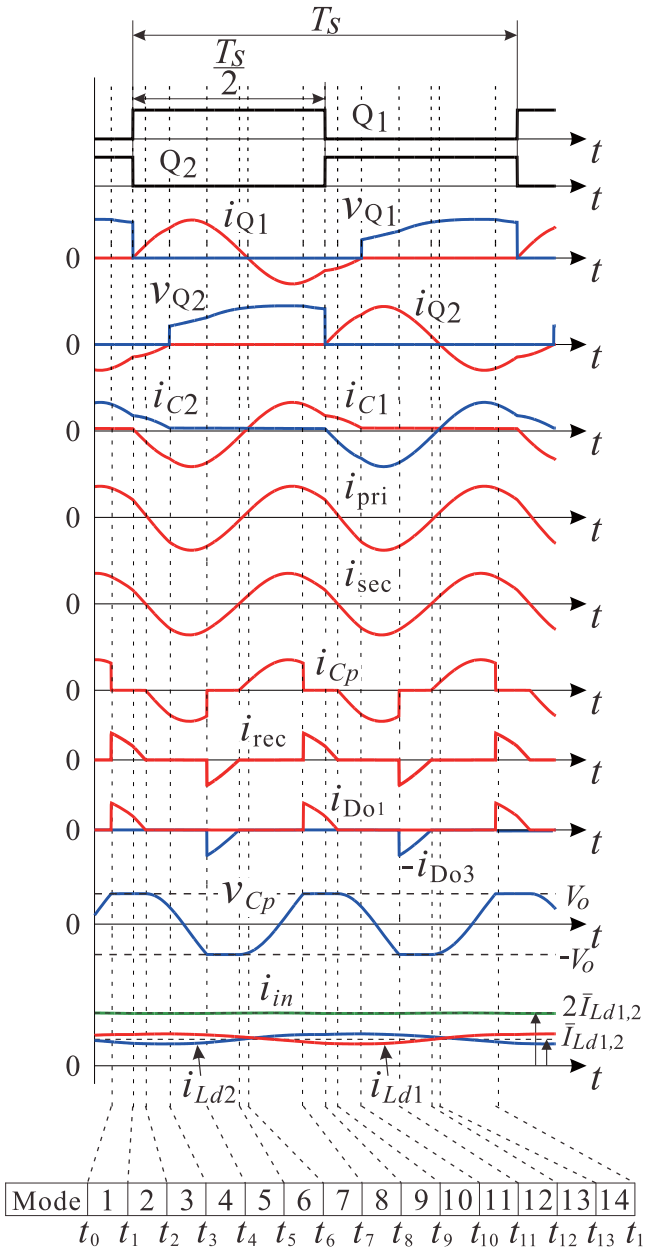

Fig. 3. Key voltage and current waveforms during one switching cycle at $\phi_s = 180°$.

$L_{s1} = L_{s2}$), the resonant capacitors C_1, C_2 ($C_n = C_1 = C_2$), and the reversely conduction type IGBTs Q_1, Q_2. The leakage fluxes between the sending and receiving coils L_1, L_2 are compensated by C_s and C_p in the primary and secondary sides respectively, thus a series-parallel (SP) compensation is employed herein. The hybrid Si-IGBT and SiC-SBD power modules are applied to Q_1 and Q_2 while the secondary-side rectifiers D_1, D_2 are comprised of Si-PNDs. It is no need to adopt SiC-SBDs for D_{o1}–D_{o4} in the secondary-side rectifiers since there is no reverse recovery current occurs by the effect of the parallel resonant tank L_2-C_p. The resonant-link capacitors C_1, C_2 contribute for blocking dc currents from L_{d1} and L_{d2} flowing into the sending coil.

The advantage of the proposed converter is applicability

This article has been accepted for publication in a future issue of this journal, but has not been fully edited. Content may change prior to final publication. Citation information: DOI 10.1109/JESTPE.2019.2927723, IEEE Journal of Emerging and Selected Topics in Power Electronics

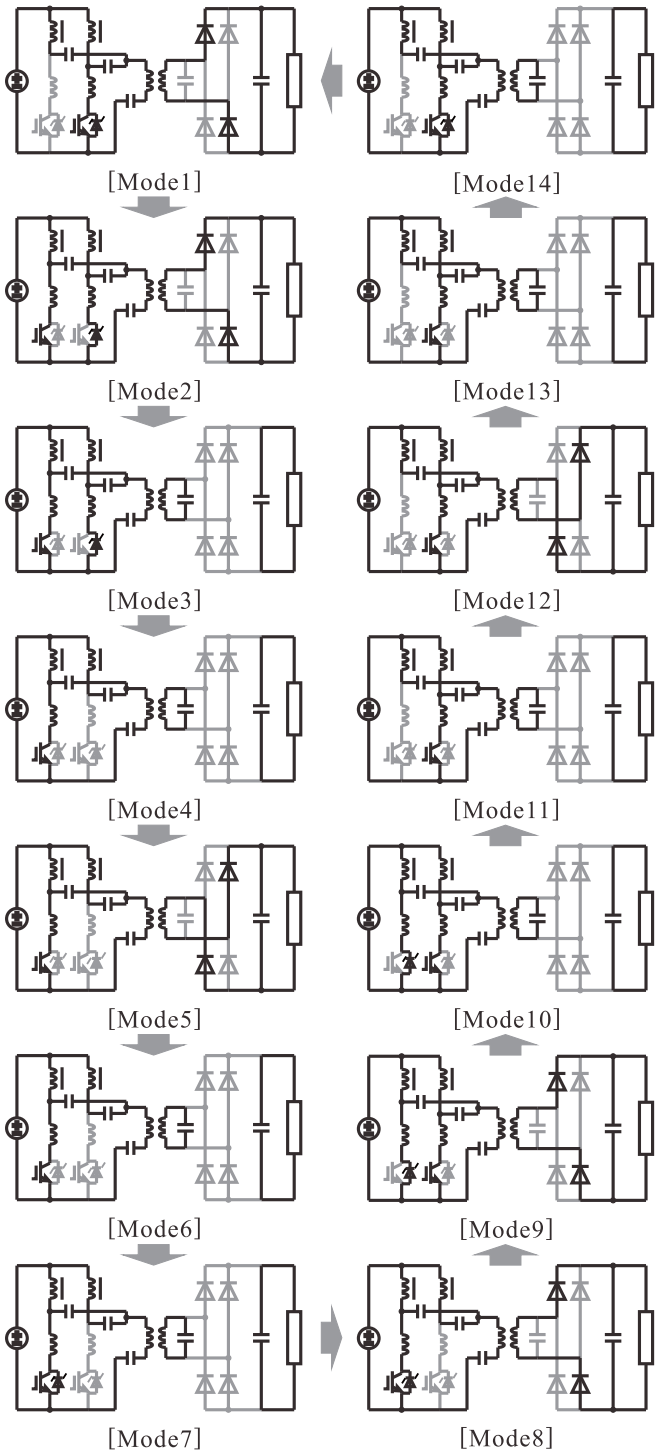

Fig. 4. Operating mode transitions and equivalent circuits during the one switching-cycle.

of time sharing principle, which is not available in the conventional class-E and class-D inverters. The high switching frequency, even MHz driving can be achieved without increasing the switching frequency and decrease of the power rating which derives from a relatively low current rating of the conventional class-E and Class-D inverters. The power rating can be increased simply by adding the phase numbers of the

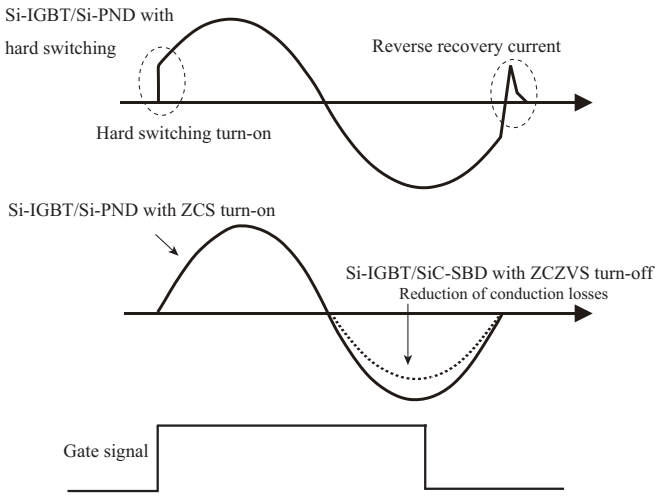

Fig. 5. Full-wave resonant current conducting through the switch and diode.

ZCS class-E inverter without losing the time sharing principle, which is also a unique feature of the proposed HF-R inverter.

The time sharing principle of the proposed HF-R inverter is based on a series load resonance on each phase. Therefore, the primary and secondary resonant tanks applicable to the proposed converters include series-series (SS) type as well as SP type. However, the resonant tank which has a compensation capacitor in parallel with L_1 such as LCC is not suitable for the proposed HF-R inverter because the series resonant link currents $i_{C1}\, i_{C2}$ will circulate within the two series resonant networks L_{s1}-C_1 and L_{s2}-C_2, thereby no power will be delivered into the sending coil brach which is in an high impedance.

The two active switches Q_1, Q_2 are driven by the interleaved gate clocking, thereby the two-phase class-E ZCS inverters U_1 and U_2 generate the two resonant link-capacitor currents i_{C_1} and i_{C_2}, respectively. The link-capacitor currents i_{C_1} and i_{C_2} are combined to produce the sending coil current i_{pri} by the time sharing manner. A single switching action yields one cycle of resonant full-wave current, the device-conducting pathway of which is divided into the active switch and anti-parallel diode.

Fig. 5 illustrates the conduction current of active switches comparatively for hard switching and ZCS. The reverse recovery current can also be reduced regardless of the type of anti-parallel diode with the aids of L_{s1} and L_{s2}. Power losses can be reduced for the reverse conduction interval of resonant current by effect of the low forward voltage of SiC-SBD. It should be remarked here ZCS is not achievable without L_1 and L_2 even if the anti-parallel diodes D_1 and D_2 are comprised of SiC-SBDs.

The ZCS operation of Q_1 and Q_2 can be achieved by the effect of L_{s1} and L_{s2}. Those small inductors attenuate a high di/dt rate at the turn-on event which is inherent to a series load resonant inverter operating with a capacitive load network [20]–[22]. In addition, the gate signals for S_1, S_2 are removed while conducting the anti-parallel diodes D_1, D_2 of Q_1, Q_2, and then zero current and zero voltage soft-switching (ZCZVS) turn-off commutation can be attained.

This article has been accepted for publication in a future issue of this journal, but has not been fully edited. Content may change prior to final publication. Citation information: DOI 10.1109/JESTPE.2019.2927723, IEEE Journal of Emerging and Selected Topics in Power Electronics

Thus, switching power losses due to the tail current inherent to the bipolar power devices can be eliminated completely.

The one switching cycle can be divided into the fourteen sub-mode intervals with ZCS commutations of the active switches and diodes as follows:

[Mode 1 ($t_0 \leq t < t_1$): Q_2 ON-state and D_{o1} & D_{o4} conducting] The series resonant current circulates in the primary-side sending coil with the anti-parallel diode D_2 of Q_2 conducting. The rectifier diodes D_{o1} and D_{o4} are forward-biased, then power is fed from the receiving coil to the load.

[Mode 2 ($t_1 \leq t < t_2$): Q_1 ZCS turn-on and Q_2 ZCZVS turn-off] The gate signal is supplied to S_1 at $t = t_1$. Accordingly, the current through Q_1 rises gradually due to the effect of L_{s1}, whereby ZCS turn-on transition starts. At the same time, the conduction current through S_2 naturally decays with the assist of L_{s2}.

[Mode 3 ($t_2 \leq t < t_3$): secondary-side diodes reversely biased and parallel compensation circuit resonates] The rectifier input current i_{rec} naturally decays to zero at $t = t_2$, then the secondary-side diodes D_{o1} and D_{o4} are reversely biased with the output voltage V_o. Accordingly, the parallel compensation circuit of the receiving coil self-inductance L_s and C_p starts to resonate.

[Mode 4 ($t_3 \leq t < t_4$): single-loop series resonance in the primary-side inverter] The current through D_2 decreases to zero with a certain slope at $t = t_3$. Thus, the reverse recover current of the anti-parallel diode can be mitigated effectively.

[Mode 5 ($t_4 \leq t < t_5$): secondary-side rectifier diodes forward-biased] The voltage across C_p builds up in the negative polarity, and reaches to $-V_o$ at $t = t_4$. Accordingly, the rectifier diodes D_{o2} and D_{o3} are forward-biased and the power is fed to the load via the receiving coil. During this interval, the parallel capacitor voltage v_{cp} are clamped to $-V_o$.

[Mode 6 ($t_5 \leq t < t_6$): secondary-side rectifier diodes reversely-biased and parallel compensation circuit resonates] The rectifier input current i_{rec} naturally decays to zero at $t = t_5$, then the secondary-side diodes D_{o2} and D_{o3} are reversely biased with the output voltage V_o. Accordingly, the parallel compensation circuit of the receiving coil self-inductance L_2 and C_p starts to resonate similarly to Mode 3.

[Mode 7 ($t_6 \leq t < t_7$): anti-parallel diode forward-biased in Q_1, and primary-/secondary-winding currents reverse direction.] The current through Q_1 decreases gradually to zero with a certain slope at $t = t_6$, and its anti-parallel diode is forward-biased. Thus, the positive half-cycle of the first full-wave appears in the sending-coil current i_{pri}. This sub-mode transition continues until v_{cp} in the secondary-side grows up to V_o at $t = t_7$.

The circuit operation from sub-mode 8 to 14 corresponds to the second full-wave interval of i_{pri}, hence the mode transitions are symmetrical to those of Sub-mode 1 to 7 as mentioned above.

B. Modeling of Sending and Receiving Coils

The sending and receiving coils of the IPT power converter can be modeled by the high frequency transformer equivalent circuit, which facilitates the analysis of the HF-link power converter for IPT[26][27].

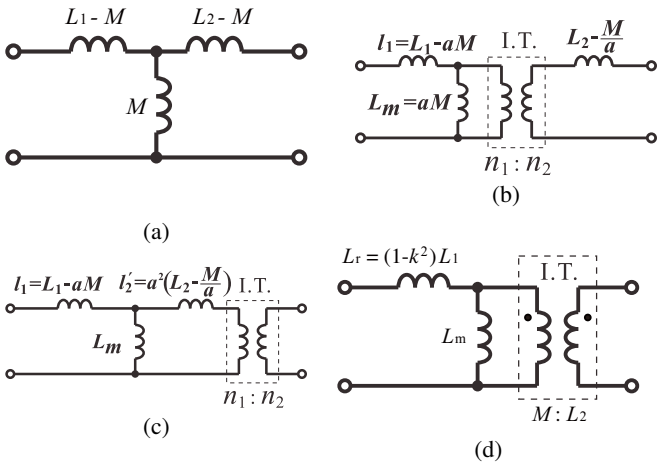

Fig. 6. HF transformer-based equivalent circuits of sending and receiving coils: (a) mutual inductor model (T-type), (b) HF-transformer model, (c) HF-transformer model with the primary-side referred secondary leakage inductance, and (d) HF-transformer model of the single leakage inductance (L-type).

The equivalent circuits of the sending and receiving coils are illustrated in Fig. 6. The self inductances L_1, L_2 consist of the main inductances L_{11}, L_{22} and the leakage inductances l_1, l_2 of the sending and receiving coils, respectively. Then, the T-type model is introduced in Fig. 6 (a) with the mutual inductance $M(= k\sqrt{L_1 L_2} = \sqrt{L_{11} L_{22}}$, k: coupling coefficient). The leakage inductances l_1, l_2 (the primary-side referred as $l_2{}'$) and magnetizing inductance L_m of the sending and receiving coils are redefined in Fig. 6 (b) and (c) as

$$l_1 = L_1 - L_{11} = L_1 - aM \quad (1)$$

$$l_2 = L_1 - L_{22} = L_2 - \frac{M}{a}, \quad l_2{}' = a^2\left(L_2 - \frac{M}{a}\right) \quad (2)$$

$$L_m = \frac{M}{L_{22}} = \frac{M^2}{L_2} = aM, \quad (3)$$

where $a(= n_1 / n_2)$ represents the windings turns ratio of ideal transformer (I.T.). Then, by assuming $l_2 = 0$ under the condition of $l_1 \neq 0$ while L_m is fixed in Fig. 6 (c), the I.T. windings turns ratio a' can be newly introduced as:

$$a' = \frac{M}{L_2} = k\sqrt{\frac{L_1}{L_2}}. \quad (4)$$

Consequently, the L-type model of the sending and receiving coils can be obtained in Fig. 6 (d) with the leakage inductance L_r redefined as:

$$L_r = (1 - k^2)L_1. \quad (5)$$

It should be notated in the modeling process that the coupling coefficient k varies in accordance with the air gap length and alignment between the two coils, which is reflected on the mutual inductance M.

C. Resonant Frequency

The series resonant frequency f_r of the series resonant network that consists of leakage inductance of the sending

This article has been accepted for publication in a future issue of this journal, but has not been fully edited. Content may change prior to final publication. Citation information: DOI 10.1109/JESTPE.2019.2927723, IEEE Journal of Emerging and Selected Topics in Power Electronics

and receiving coils, link capacitor and ZCS-assisted inductor in each phase can be defined by

$$f_r = \frac{1}{2\pi\sqrt{L_c C_r}} \tag{6}$$

$$L_c = L_s + L_r, \quad C_r = \frac{C_n \cdot C_s}{C_n + C_s}. \tag{7}$$

In order to perform the ZCS turn-on of active switches and ZCS turn-off of parallel diodes, the switching frequency f_s is selected as

$$f_s = \frac{f_o}{2} > \frac{f_r}{2}, \tag{8}$$

where f_o represents the sending coil current frequency. As a result, a higher frequency resonant current can be produced efficiently to the sending coil while suppressing the switching frequency. In addition, all the diodes of the secondary-side rectifier are also commutated in ZCS due to the primary-side series and secondary-side parallel (SP) compensation resonant tanks. Adoption of the SP compensation can be justified by considering the voltage boost function of the current-fed ZCS HF-R inverter [23]. The parallel resonant frequency f_p can be defined by

$$f_p = \frac{1}{a'} \cdot \frac{1}{2\pi\sqrt{(1-k^2)L_1 C_p}} \tag{9}$$

where M denotes the mutual inductances of sending and receiving coils, a' and k represent the winding turns ratio and the coupling coefficient of the ideal transformer, respectively.

III. Power Control Method

A constant switching frequency pulse modulation is essential to the effective power transmission of an IPT resonant converter. In order to carry out the output power control of the proposed converter, PSM of the two-phase active switches Q_1 and Q_2 is applied under the condition of constant switching frequency [24][25].

The phase difference between the gate signals of Q_1 and Q_2 is reduced from 180° as shown in Fig.7(a),(b) on the basis of the PSM principle. This pulse modulation enables the RMS value of the HF-R inverter current adjust continuously to the load impedance variations, thereby the output power control is achievable under the high frequency condition. In this case, the phase angle ϕ_s of the gate signal is defined as

$$\phi_s = \frac{t_{\phi_s}}{T_s} \times 360\,[^\circ]. \tag{10}$$

The DC output power can be controlled by adjusting ϕ_s, whereby simplification of the power circuit and control system can be attained as compared to other power regulation schemes such as pulse amplitude modulation (PAM).

The continuous resonant current i_{pri} appears during the interval from the turn-on of S_1 to the turn-off of S_2 as illustrated in Fig. 7. Therefore, ZCS turn-on and ZCZVS turn-off operations of the fixed-phase switch Q_1 can attain for all the range of PS angle ϕ_s by the effect of i_{pri}. On the other hand, the primary-side sending coil current i_{pri} becomes discontinuous during the interval from the turn-on of D_1 to the end of the cycle ($t_{D2,on} \rightarrow T_s$). Accordingly, ZCS turn-on of the controlled and lagging-phase switch Q_2 can attain at any

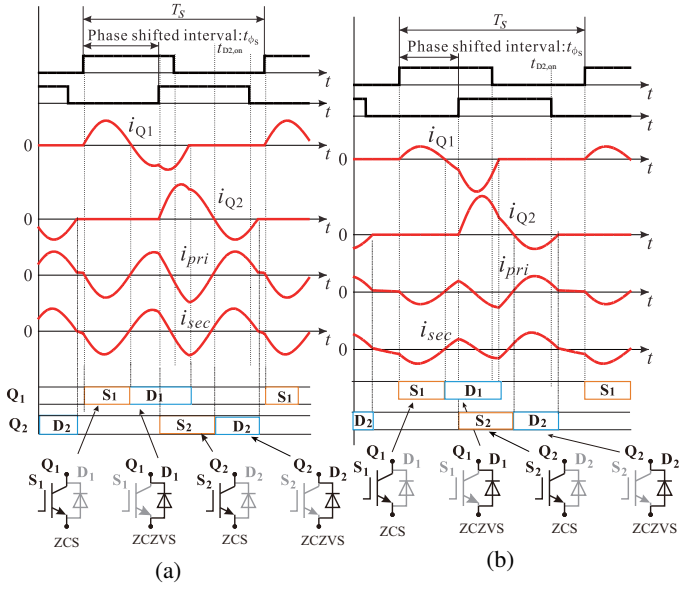

Fig. 7. PSM pulse patterns and key current waveforms: (a) $\phi_s = 150°$, and (b) $\phi_s = 115°$.

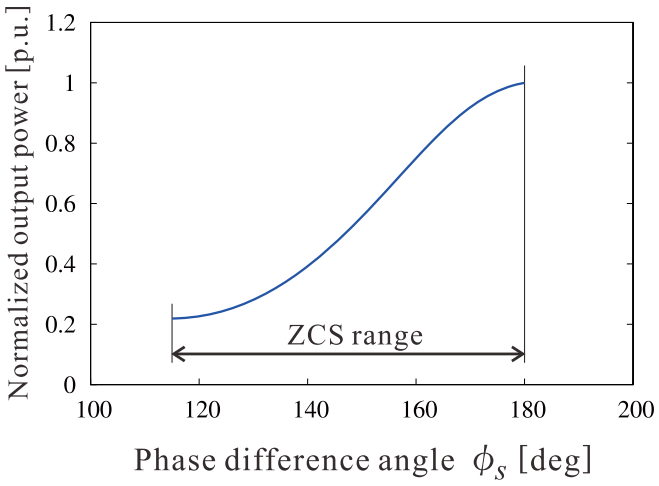

Fig. 8. Simulated output power versus phase difference angle curves.

set of ϕ_s, while its ZCZVS turn-off operation is subject to the condition for ensuring the forward bias of D_2 as:

$$\int_{t_{D2,on}}^{T_s} i_{pri} dt > 0. \tag{11}$$

The simulated power control characteristics by PSM of the proposed IPT converter is depicted in Fig.8 with the same parameters of prototype experiment as after mentioned. The output power is continuously controlled from the rated power to the minimum power by PSM. Additionally, ZCS turn-on and ZCZVS turn-off transitions can be ensured in all the switches. It can be seen from Fig.7 that the double frequency component of the sending and receiving coil currents are reduced in accordance with reduction of ϕ_s, and eventually the switching frequency component is dominant.

The harmonic analysis of sending and receiving coil currents is demonstrated by simulation to determine the control

This article has been accepted for publication in a future issue of this journal, but has not been fully edited. Content may change prior to final publication. Citation information: DOI 10.1109/JESTPE.2019.2927723, IEEE Journal of Emerging and Selected Topics in Power Electronics

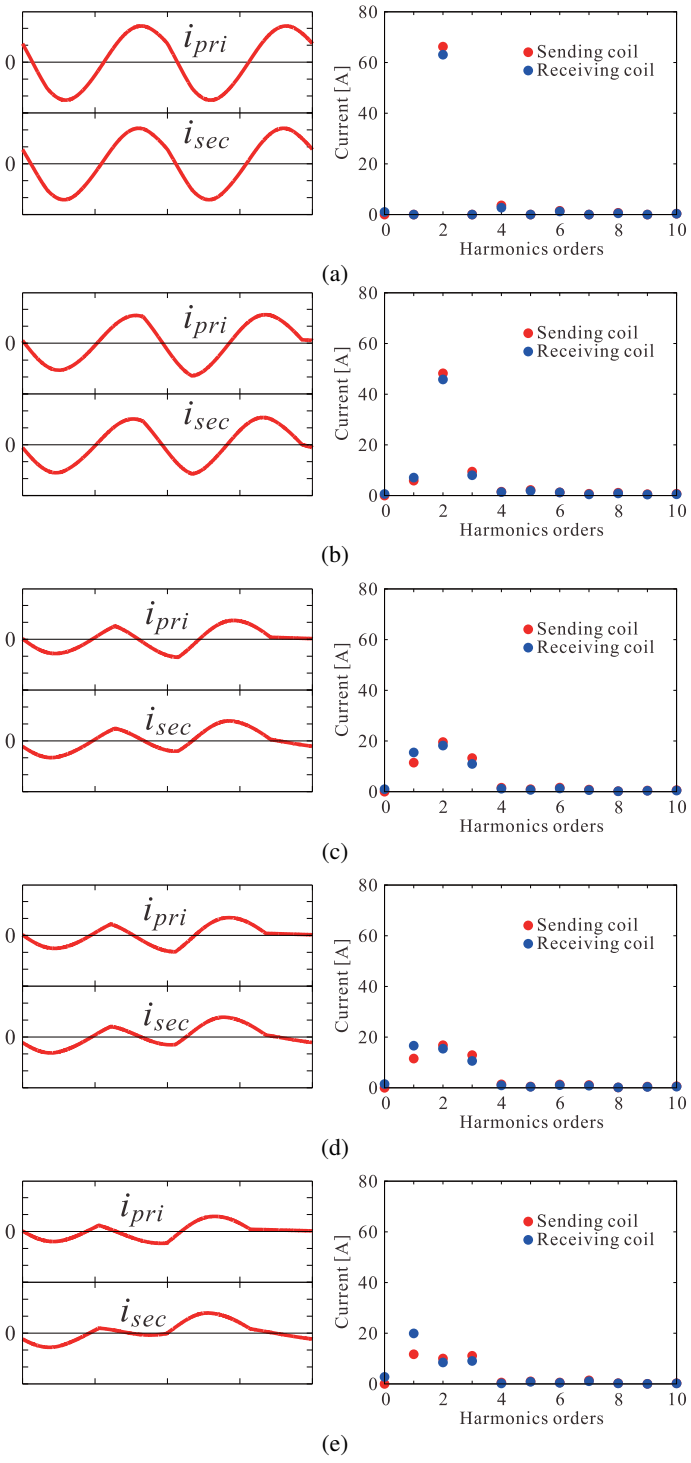

Fig. 9. Simulated sending and receiving coils current waveforms with FFT analysis under the various output power conditions: (a) $\phi_s = 180°$, (b) $\phi_s = 150°$, (c) $\phi_s = 115°$, (d) $\phi_s = 110°$, and (e) $\phi_s = 95°$ (30 A/div, 5 μs/div).

range of ϕ_s. Sending and receiving coil current waveforms and Fast Fourier Transform (FFT) harmonic analysis results are depicted in Fig.9 (a)–(e). The double frequency component keeps at a high value, compared to the switching frequency component in the range of $\phi_s = 115°$–$180°$. The switching

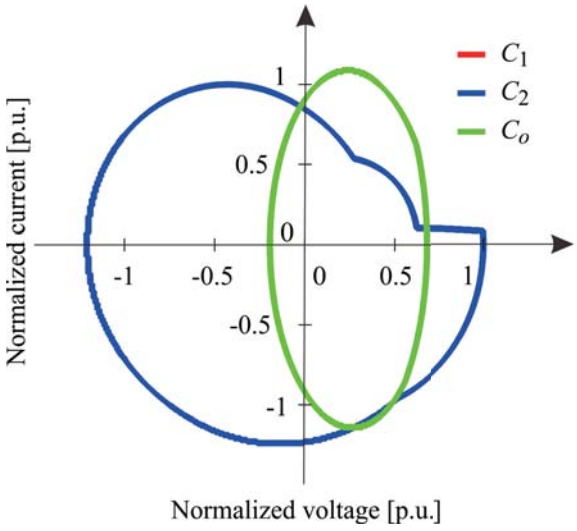

Fig. 10. State plane trajectories at $\phi_s = 180°$.

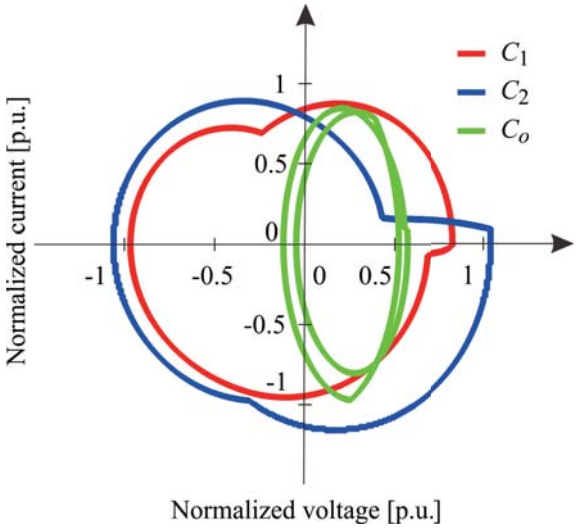

Fig. 11. State plane trajectories at $\phi_s = 150°$.

frequency component of the receiving coil current i_{sec} exceeds the double frequency components at $\phi_s = 110°$. Additionally, the switching frequency component completely overwhelms the double frequency component both in i_{pri} and i_{sec} at $\phi_s = 95°$. This result implies that there is no generating the double frequency component for the load resonant current less than $\phi_s = 95°$. The simulation analysis which is demonstrated herein justifies the phase angle range setting to $\phi_s = 115°$–$180°$ in the experimental verification as mentioned in the next section.

In order to observe the inductive and capacitive energies inside the resonant tanks, the state-plane trajectories are investigated by simulation in accordance with the variations of ϕ_s. Fig. 10 indicates the trajectories of each resonant capacitors C_1, C_2 and C_o with $\phi_s = 180°$. The two-phase ZCS HF-R inverters have the identical trajectory which exceeds that of the sending coil. This implies that the resonant tanks operate equally for delivering the same energies to the sending

This article has been accepted for publication in a future issue of this journal, but has not been fully edited. Content may change prior to final publication. Citation information: DOI 10.1109/JESTPE.2019.2927723, IEEE Journal of Emerging and Selected Topics in Power Electronics

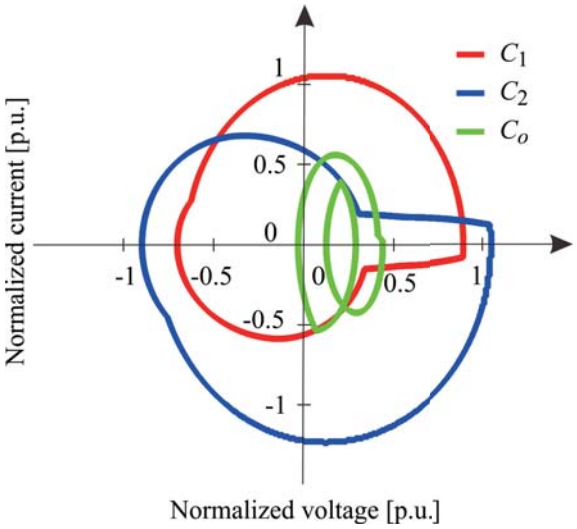

Fig. 12. State plane trajectories at $\phi_s = 115°$.

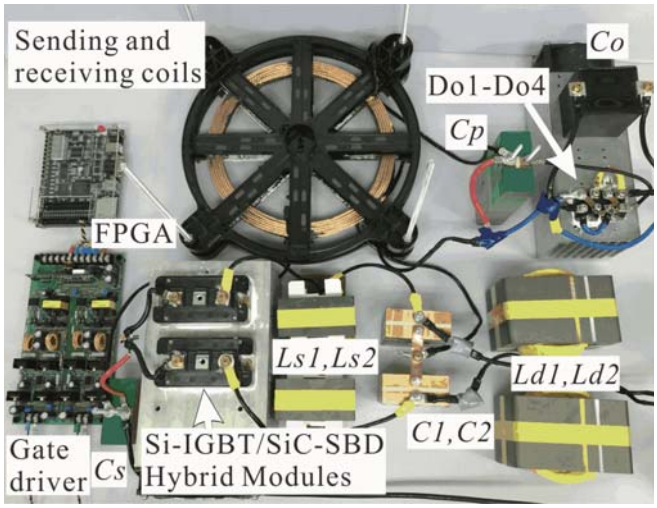

Fig. 13. Exterior appearance of the IPT power converter prototype.

coil. The state-plane trajectory of the fixed HF-R inverter with Q_1 gradually exceeds over that of the controlled-phase ZCS HF-R inverter with Q_2 as indicated in Figs. 11 and 12 with $\phi_s = 150°$ and $115°$. In addition, difference begins to appear between first and second circular traces of i_{pri}, which derives from the small distortions of current waveforms in Figs. 9 (b) and (c). It can also be known from the state plane analysis that the voltage stress of the primary-side series compensation capacitor C_o is reduced by the effects of C_1 and C_2. Accordingly, the design consideration on the sending and receiving coils together with the series compensation circuits should have importance on the current rating rather than the voltage stress in the proposed IPT converter.

IV. Experimental Results and Discussions

A. Experimental Set-Up and Specification

The practical feasibility of the proposed IPT power converter is investigated by experiment on a 2.0 kW-100 kHz laboratory prototype. The exterior appearance of the prototype and experimental setup is depicted in Fig. 13. The trench-gate Si-IGBT / SiC-SBD hybrid power module *CM100DY-24NFH* (1200 V, 100 A, V_{CEsat} :5.0 V, V_{EC}: 1.7 V, Mitsubishi) is implemented in the prototype while the secondary-side rectifier D_{o1}-D_{o2} consist of Si-PND *DSEI 2x31-10B* (600 V, 2×30 A, IXYS), as shown in Fig. 14. The package of hybrid module has compatibility with a conventional two-in-one power module, therefore the gate driver and layout design of Si-IGBT power module can be applied for the prototype.

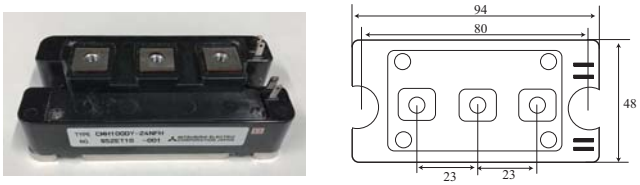

(a) (b)

Fig. 14. High speed Si-IGBT/SiC-SBD hybrid power modules: (a) appearance, and (b) schematic diagram (scale unit:mm).

TABLE I. Experimental Circuit Parameters

Item	Symbol	Value[unit]
Output power rating	P_o	2 [kW]
Input voltage	V_{in}	170 [V]
Output voltage	V_o	192 [V]
DCLs	L_{d1},L_{d2}	500 [μH]
ZCS-assisted inductors	L_{s1},L_{s2}	7 [μH]
Resonant capacitors	C_1,C_2	300 [nF]
Power factor tuned capacitor	C_s	600 [nF]
Parallel resonant capacitor	C_p	390 [nF]
Load resistor	R_o	18 [Ω]
Switching frequency	f_s	50 [kHz]
HF-R inverter output frequency	f_o	100 [kHz]
Series resonant frequency	f_r	86 [kHz]
Parallel resonant frequency	f_p	99 [kHz]
Sending and receiving coils		
Self inductance of sending coil	L_1	22.4 [μH]
Self inductance of receiving coil	L_2	22.4 [μH]
Mutual inductance	M	16.5 [μH]
Coupling coefficient of L_1 and L_2	k	0.74
$*$ Winding turns of L_1 and L_2	N_1/N_2	6/6 [turn]
$*$ Air gap length of L_1 and L_2	g	10 [mm]
Litz wire 7/14/2UEM, Ishizue Magnet Wire Works Ltd.		

Specification of the prototype including the sending and receiving coils are indicated in TABLE I. It should be noted here that the switching and resonant frequencies are based on the self-inductances L_1, L_2 of the sending and receiving coils that are measured at the gap-length $g = 10\,\mathrm{mm}$. Once the sending coil frequency f_o is set to 100 kHz, the switching frequency can be determined to 50 kHz in accordance with the time-sharing principle. Hence, the loaded resonant frequency f_r is selected to 86 kHz with consideration for (8). The sending and receiving coils are implemented with Litz wires (44 twists / 7 bundles of $0.2\,\mathrm{mm}^2$ cross section).

B. Steady-State Performances

The observed switching waveforms of Q_1, Q_2, sending and receiving coils as well as the rectifier diode are depicted in Figs.15 and 16 for the rated output power at $\phi_s = 180°$.

This article has been accepted for publication in a future issue of this journal, but has not been fully edited. Content may change prior to final publication. Citation information: DOI 10.1109/JESTPE.2019.2927723, IEEE Journal of Emerging and Selected Topics in Power Electronics

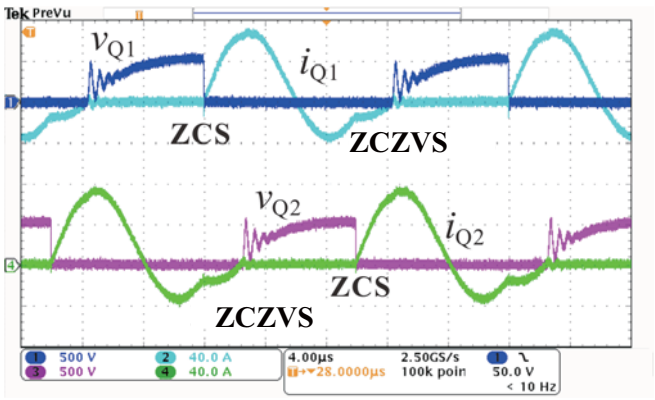

Fig. 15. Observed switching voltage and current waveforms at $\phi_s = 180°$, $P_o = 2.0\,\mathrm{kW}$ (500 V/div, 40 A/div, 4 µs/div).

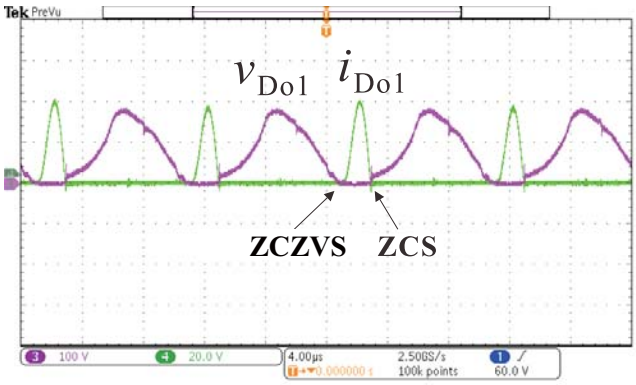

Fig. 16. Observed voltage and current of rectifier a diode at $\phi_s = 180°$, $P_o = 2.0\,\mathrm{kW}$ (100 V/div, 20 A/div, 4 µs/div).

The ZCS turn-on and turn-off commutations can be confirmed for Q_1 and Q_2 in Fig.15. The ZCS turn-on and turn-off are also achieved in the secondary-side rectifier diode as shown in Fig. 16 due to effect of the parallel resonant tank in the secondary side. Fig.17 exhibits the resonant currents i_{pri} and i_{sec} in phase, which proves the effective power transfer achieves successfully between the sending and receiving coils in the proposed IPT power converter.

Voltage-ringing operations appear in the active switches at their turn-off transitions as observed in Figs. 15, 18 and 21. Those phenomena are caused by the oscillation of the parasitic output capacitance C_{os} of active switch in the hybrid power module and the ZCS-assisted inductors L_{s1}, L_{s2} together with the stray inductance L_r[28]. The ringing interval t_p is expressed as

$$t_p = \frac{2\pi}{\sqrt{\frac{1}{L_s C_{os}} - \left(\frac{r_l}{2L_r}\right)^2}}. \tag{12}$$

Accordingly, the switching noise and ringing can be mitigated by minimizing the parasitic capacitances and stray inductance of the Si-IGBT / SiC-SBD hybrid module, which is one of the future challenges of the proposed converter from the viewpoint of packaging and wire-bonding technologies.

The ZCS commutations and power transfer can also be

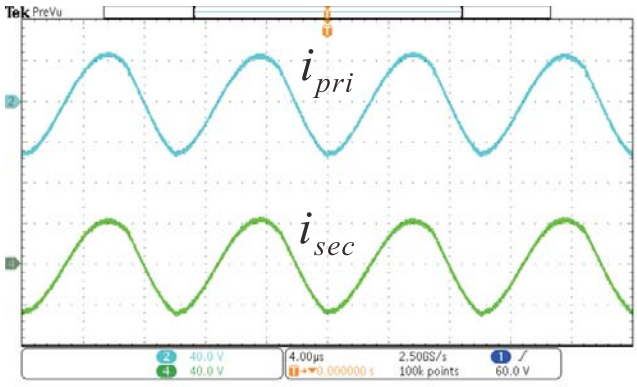

Fig. 17. Observed current waveforms of sending and receiving coils at $\phi_s = 180°$, $P_o = 2.0\,\mathrm{kW}$ (40 A/div, 4 µs/div).

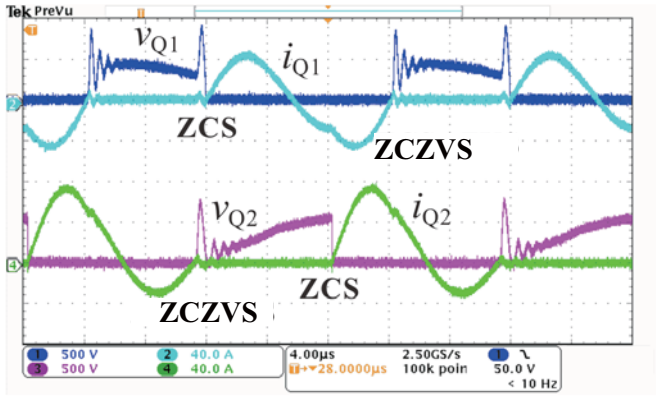

Fig. 18. Observed switching voltage and current waveforms at $\phi_s = 150°$, $P_o = 1.15\,\mathrm{kW}$ (500 V/div, 40 A/div, 4 µs/div).

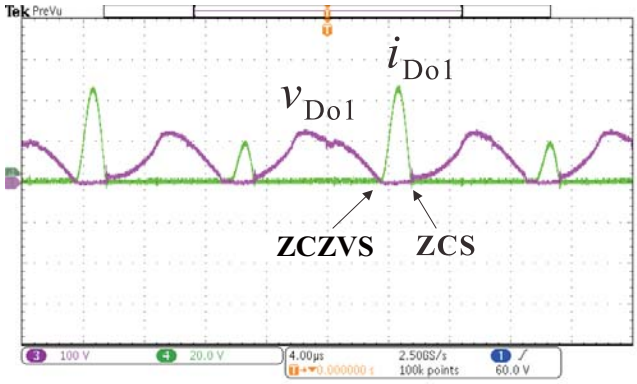

Fig. 19. Observed voltage and current of rectifier a diode at $\phi_s = 150°$, $P_o = 1.15\,\mathrm{kW}$ (100 V/div, 20 A/div, 4 µs/div).

observed at $\phi_s = 150°$ in Figs.18 and 19. The sending and receiving coil currents get into the boundary condition of continuous and discontinuous conduction modes as depicted in Fig. 20. This implies the switching frequency component emerges in the sending and receiving coils currents.

The ZCS commutations of the active switches and diodes still maintain at $\phi_s = 115°$ in Figs.21 and 22. The half-cycle waveforms of i_{Q_1} and i_{Q_2} are canceled out each other,

This article has been accepted for publication in a future issue of this journal, but has not been fully edited. Content may change prior to final publication. Citation information: DOI 10.1109/JESTPE.2019.2927723, IEEE Journal of Emerging and Selected Topics in Power Electronics

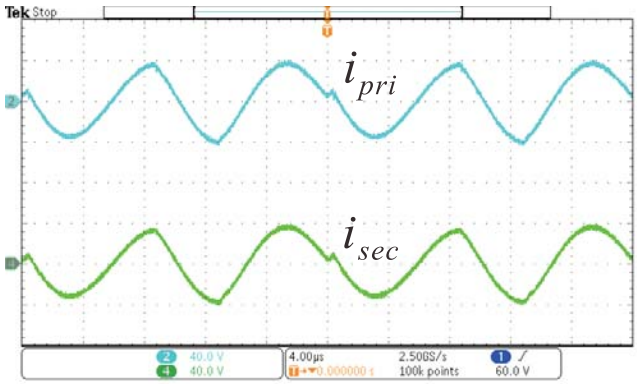

Fig. 20. Observed current waveforms of sending and receiving coils at $\phi_s = 150°$, $P_o = 1.15\,\mathrm{kW}$ ($40\,\mathrm{A/div}$, $4\,\mu\mathrm{s/div}$).

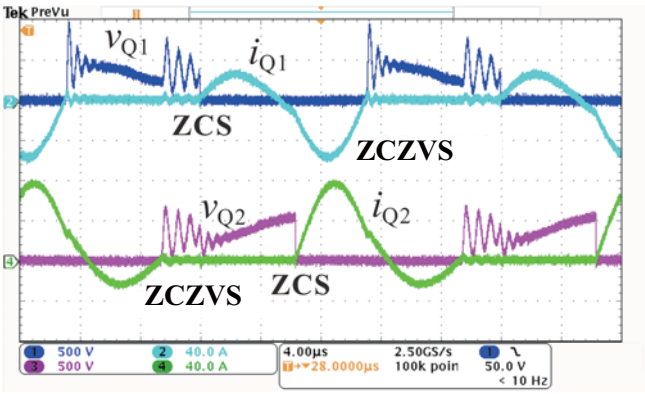

Fig. 21. Observed switching voltage and current waveforms at $\phi_s = 115°$, $P_o = 440\,\mathrm{W}$ ($500\,\mathrm{V/div}$, $40\,\mathrm{A/div}$, $4\,\mu\mathrm{s/div}$).

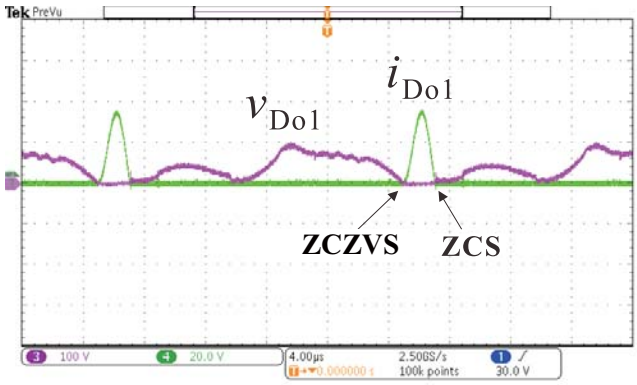

Fig. 22. Observed voltage and current of rectifier a diode at $\phi_s = 115°$, $P_o = 440\,\mathrm{W}$ ($100\,\mathrm{V/div}$, $20\,\mathrm{A/div}$, $4\,\mu\mathrm{s/div}$).

consequently the sending and receiving-coils currents, i_{pri} and i_{sec} contain a small amount of dc component while keeping the double frequency principle as depicted in Fig. 23. It should be remarked herein that the high frequency magnetizing current, which is identical to the circulating current between the sending and receiving coils, can be minimized regardless of ϕ_s owing to the effect of the SP compensation circuit.

The steady-stage characteristics of output power and phase

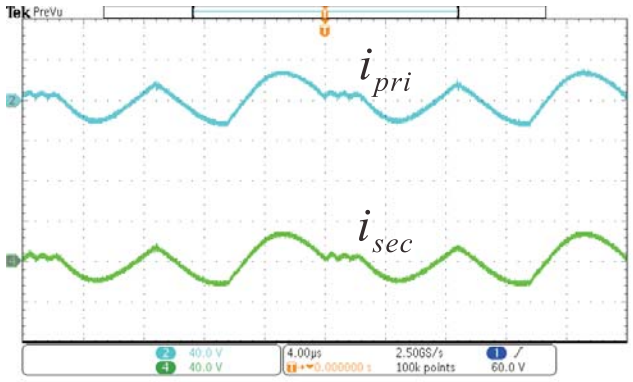

Fig. 23. Observed current waveforms of sending and receiving coils at $\phi_s = 115°$, $P_o = 440\,\mathrm{W}$ ($40\,\mathrm{A/div}$, $4\,\mu\mathrm{s/div}$).

difference angle are indicated together with the ZCS range in Fig. 24. The output power is regulated from the rating $2.0\,\mathrm{kW}$ to minimum $440\,\mathrm{W}$ at $\phi_s = 115°$, thus the validity of PSM-based high frequency power regulation is actually demonstrated for the IPT power converter.

The proposed IPT converter can accommodate larger gap lengths such as $100\,\mathrm{mm}$-$150\,\mathrm{mm}$ by introducing a multi-resonant tanks such as $LCCL$ in the secondary side [29], while the series compensation resonant tank maintains in the primary side for attaining the time sharing principle.

C. Power Loss Analysis

The actual power conversion efficiencies of the prototype are provided in Fig. 25. The three stages of power conversion efficiencies are measured including the power transmission efficiency between the receiving and sending coils: efficiency from the dc input to the inverter output stage as $\eta_{HF,i}$ ($= \frac{\overline{v_{L1} i_{pri}}}{V_{in} i_{in}}$), the high frequency output (rectifier input) stage as $\eta_{HF,o}$ ($= \frac{\overline{v_{cp} i_{rec}}}{V_{in} i_{in}}$), and the dc output stage as $\eta_{DC,o}$ ($= \frac{\overline{V_o i_o}}{V_{in} i_{in}}$), respectively. Note here the controller power consumption is not considered in the measurement. The maximum efficiency of $\eta_{DC,o}$ records as $79.0\,\%$ at $P_o = 2.0\,\mathrm{kW}$, while $91.0\,\%$ and $81.0\,\%$ achieve in $\eta_{HF,i}$ and $\eta_{HF,o}$ respectively.

The loss breakdown for the dc-dc power conversion efficiency $\eta_{DC,o}$ is exhibited in Fig. 26. The indexes in the graph are as follows: active switches S_1, S_2 conduction losses P_{S_1}, P_{S_2}, anti-parallel diodes D_1, D_2 conduction losses P_{D_1}, P_{D_2}, secondary-side rectifier diodes conduction total losses P_D, DCLs L_{d1}, L_{d2} total power loss P_{L_d}, ZCS-assisted inductors L_{s1}, L_{s2} total losses P_{L_s}, sending coil conduction losses P_{L1}, receiving coil conduction loss P_{L2}, primary-side capacitors C_1, C_2 and C_s total power losses P_{Cr}, and output capacitor losses P_{Co}. The switching power losses of all the power devices of the primary and secondary-sides can be minimized over the whole power range due to the effect of the wide-range ZCS commutations deriving from the proposed circuit topology. The other loss (approximately $5\,\%$ of the total loss) includes the wire and connector losses on top of the iron power loss of the ferrite cores of sending and receiving coils. The copper losses of the sending and receiving coils account for a large portion of the total power loss at the rated power. Therefore, the efficiency

This article has been accepted for publication in a future issue of this journal, but has not been fully edited. Content may change prior to final publication. Citation information: DOI 10.1109/JESTPE.2019.2927723, IEEE Journal of Emerging and Selected Topics in Power Electronics

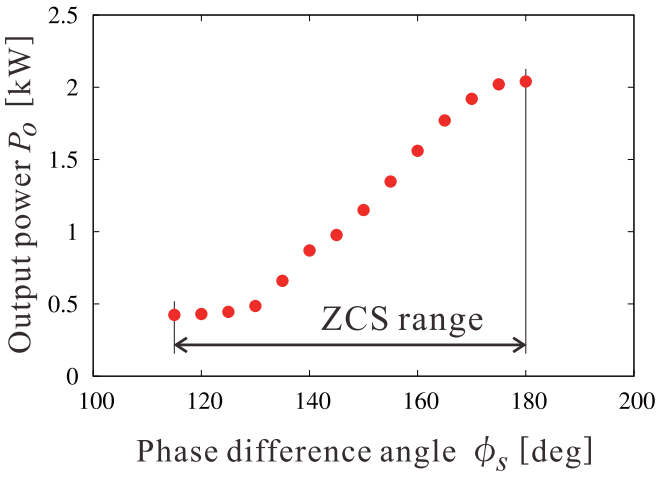

Fig. 24. Experimental output power versus phase difference angle curves.

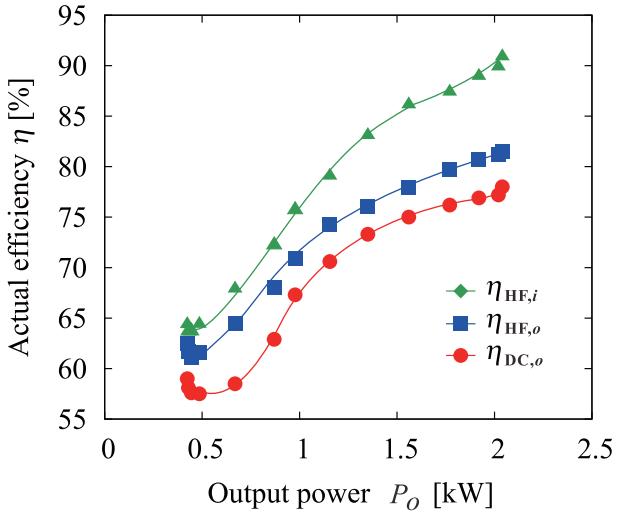

Fig. 25. Actual efficiencies of inverter output, high frequency output and DC output stages.

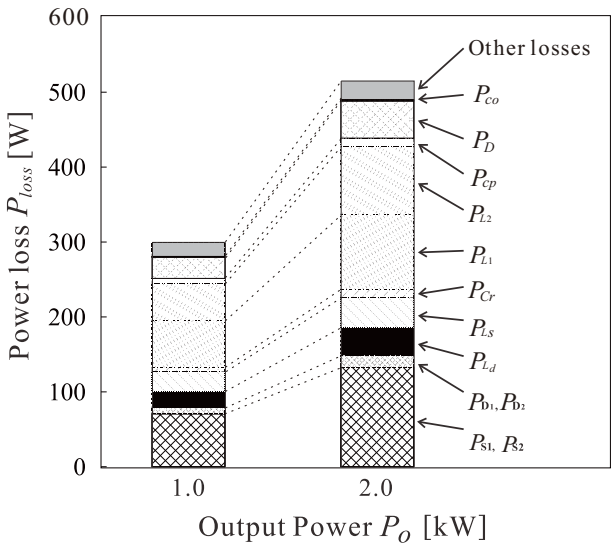

Fig. 26. Measured power loss analysis.

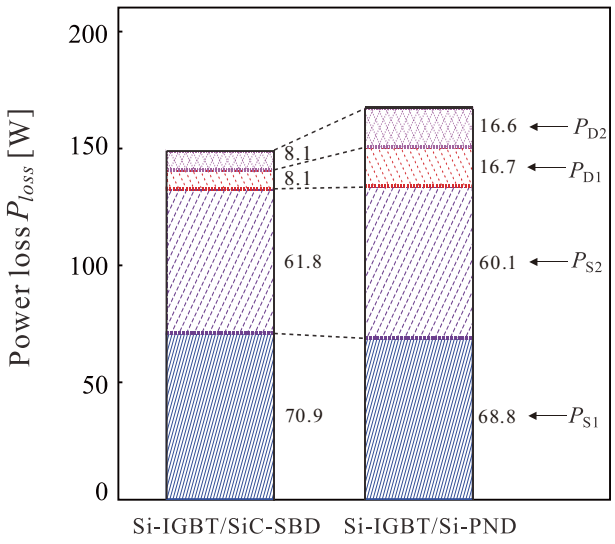

Fig. 27. Comparison of power loss breakdown.

will improve by optimizing the sending and receiving coils together with the ferrite materials and structure.

In order to confirm the effect of the Si-IGBT / SiC-SBD hybrid power module, the power loss analysis of the inverter is indicated in Fig. 27 as compared with the case of using Si-IGBT / Si-PND power module *CM100DU-24NFH* (1200 V, 100 A, V_{CEsat} :5.0 V, V_{EC}: 3.5 V, Mitsubishi). It can be confirmed from this analysis that the power loss of the reverse conduction to anti-parallel diode is approximately halved by applying a SiC-SBD. As a result, the power conversion efficiency $\eta_{HF,i}$ from the DC input to HF-R inverter with the Si-IGBT / SiC-SBD power module improves to 91 % from 90 % of the prototype with the Si-IGBT / Si-PND power module. The largest parts of power loss breakdowns are P_{S_1}, P_{S_2} regardless of the anti-parallel diode. This breakdown derives from the derating of power module voltage for accommodating the voltage stress due to the parasitic ringing as discussed in the previous subsection with (12). By reducing the parasitic inductances and capacitances in the power module, the higher power conversion efficiencies will improve at any stage of power conversions.

V. Conclusions

A time-sharing current-fed ZCS high frequency resonant inverter-applied resonant dc-dc converter for inductive power transfer applications has been proposed and evaluated by theoretical and experimental analyses. It has been clarified by experimental results that high frequency current generation with ZCS commutations can be achieved under the time sharing principle, which is suitable for bipolar switching power devices. A 100 kHz resonant current has been successfully produced in the two-phase current-fed high-frequency inverters at the half frequency of 50 kHz. The resonant current phasor control has been verified under the condition of constant frequency, whereby the continuous power control from 2 kW-0.5 kW has achieved. The reversely conducting power loss has decreased almost by half owing to the effect SiC-SBD

in the anti-parallel diode of the hybrid power module. The dc-HFAC power conversion efficiency attains $91\,\%$ while the dc-dc conversion is about $80\,\%$ at the dc output power $P_o = 2\,\mathrm{kW}$. All the research results verify the effectiveness of the proposed converter and power control schemes for inductive power transfer systems.

The output frequency f_o is set as $100\,\mathrm{kHz}$ just for facilitating the evaluations on the remarkable characteristics of the proposed converter, while the standard switching frequency of EV IPT wireless battery charger is offered as $85\,\mathrm{kHz}$ by the guideline SAE J2954. The feasibility of the proposed converter with the time sharing principle can also be verified for the standard frequency-applied system.

The future research topics include evaluations of the proposed IPT converter for larger gap lengths of the sending and receiving coils that corresponds with the EV guideline SAE J2954 by adopting the multi-resonant tank as well as optimizing the design of the coil structure.

REFERENCES

[1] A. Bindra, "Wide-bandgap power devices, *adoption gathers momentum*," *IEEE Power Electron. Magz.*, vol.2, no.2, pp.42-47, Mar. 2015.

[2] M. Johnson, P.R. Wilson, L. Empringham, and L. De Lillo, "IEEE ITRW working group position paper-packaging and integration, *unlocking the full potential of wide-bandgap devices*," *IEEE Power Electron. Magz.*, vol.5, no.2, pp.22-25, Jun. 2018.

[3] G.A. Covic, and J.T. Boys, "Modern trends in inductive power transfer for transportation applications," *IEEE J. Emerg. Sel. Topics in Power Electron.*, vol.1, no.1, pp.28-41, Jul. 2013.

[4] S. Li and C. Mi, "Wireless power transfer for electric vehicle applications," *IEEE J. Emerg. Sel. Topics in Power Electron.*, vol.3, no.1, pp.4-16, Mar. 2015.

[5] H.A. Mantooth, M.D. Glover, and P.-Shepherd, "Wide bandgap technologies and their applications on miniaturizing power electronics systems," *IEEE J. Emerg. Sel. Topics in Power Electron.*, vol.2, no.3, pp.374-385, Sep. 2014.

[6] M. Fernãndez, X. Perpiñà, J. Roing-Guitart, M. Vellvehi, F. Bauwens, M. Tack, and X. Jordà, "Short-circuit study in medium-voltage GaN cascodes, p-GaN HEMTs, and GaN MISHEMTs," *IEEE Trans. Ind. Electrons.*, vol.64, no.11, pp.9012-9021, Nov. 2017.

[7] E.A. Jones, F. Wang, and D. Constinett, "Review of commercial GaN power devices and GaN-based converter challenges," *IEEE J. Emerg. Sel. Topics in Power Electron.*, vol.4, no.3, pp.707-719, Sep. 2016.

[8] R.R. Potera and T.J. Han, "Silicon carbide diodes in power factor correction circuits," *IEEE Power Electron. Magz.*, vol.6, no.2, pp.34-39, Mar. 2019.

[9] N. Oswald, P. Anthony, and N. McNeill, and B.H. Stark, "An experimental investigation on the tradeoff between switching losses and EMI generation with hard-switched all-Si, Si-SiC, and all-SiC device combinations," *IEEE Trans. Power Electron.*, vol.29, no.5, pp.2393-2407, May 2014.

[10] B. Zhao, Q. Song, and W. Liu, "Experimental comparison of isolated bidirectional dc-dc converters based on all-Si and all-SiC power devices for next-generation power conversion application," *IEEE Trans. Ind. Electrons.*, vol.61, no.3, pp.1389-1393, Mar. 2014.

[11] S. Samanta, A.K. Rathore, and D.J. Thrimawithana, "Analysis and design of current-fed half-bridge (*C*)(*LC*)-(*LC*) resonant topology for inductive wireless power transfer application," *IEEE Trans. Ind. Appl.*, vol.53, no.4, pp.3917-3926, Jul./Aug., 2017.

[12] S. Samanta, A.Kumar. Rathore, and S.K. Sahoo, "Concept study and feasibility analysis of current-fed power electronics for wireless power transfer system, *Proc. 2016 IEEE Intnl Conf. Power Electron. Drives and Energy Sys.* (PEDES), pp.1-6.

[13] N.R. Reddi, M.R. Ramteke, H.M. Suryawanshi, K. Kathapalli, and S.P. Gawanda, "An isolated multi-input ZCS dc-dc front-end-converter based multilevel inverter for the integration of renewable energy sources," *IEEE Trans. Ind. Appli.*, vol.54, no.1, pp.494-504, Jan./Feb., 2018.

[14] G.A. Covic, and J.T. Boys, "Inductive power transfer," *Proc. The IEEE*, vol.101. no.6, pp.1276-1289, Jun. 2013.

[15] B. Yuan, X. Yang, D. Li, Y. Pei, J. Duan, and J. Zhai, "A current-fed multiresonant converter with low circulating energy and zero-current switching for high step-up power conversion.", *IEEE Trans. Power. Electron.*, vol.26, no.6, pp.1613-1619, Jun. 2011.

[16] U.K. Madawala and D.J. Thrimawithana, "Current-sourced bi-directional inductive power transfer," IET Power Electron., vol.4, no.4, pp.471-480, May 2011.

[17] C. Zheng, R. Chen, E. Faraci, Z.U. Zahid, M. Senesky, D. Anderson, J. Lai, W. Yu, and C. Lin, "High efficiency contactless power transfer system for electric vehicle battery charging." *Proc. 2013-ECCE*, pp.3243-3249, Sep. 2013.

[18] N.M. Vietson, M. Nakaoka, and T. Maruhashi, "Analysis of current-fed-type high frequency inverter using a single reversely-conducting thyristor," *IEEE Trans. Ind. Electron. Contr. Instrum.*, vol.IECI-26, no.1, pp.35-39, Feb. 1979.

[19] T. Mishima, K. Konishi, and M. Nakaoka, "Current-source ZCS high-frequency resonant inverter based on time-sharing frequency doubler principle and its induction heating applications." *Proc. IEEE Power Electronics and Drive Systems Conf.* (PEDS) 2015, pp.598-603, Jun. 2015.

[20] J.G. Kassakian, "A new current mode sine wave inverter," *IEEE Trans. Ind. Appl.*, vol. IA-18, no.3, pp.273-278, May/Jun. 1982.

[21] N. Sanajit, and A. Jangwanitlert, "A series-resonant half-bridge inverter for induction-iron appliances," *Proc. 2011 IEEE Power Electronics and Drive Systems Conf.* (PEDS), pp.46-50, Dec. 2011.

[22] R.W. Erickson and D. Maksimović, "Fundamentals of power electronics – second edition," Kluwer Academic Publications, ISBN:0-7923-7270-0, 2004.

[23] J. Hou, Q. Chen, K. Yan, X. Ren, S. Wong, and Chi.K Tse, "Analysis and control of S/SP compensation contactless resonant converter with constant voltage gain." *Proc. 2013-ECCE*, pp.2552-2558, Sep. 2013.

[24] T. Mishima and M. Nakaoka, "A load-power adaptive dual pulse modulated current phasor-controlled ZVS high-frequency resonant inverter for induction heating applications," *IEEE Trans. Power Electron,*, vol.29, no.8, pp.3864-3880, Aug. 2014.

[25] T. Mishima, C. Takami, and M. Nakaoka, "A new current phasor-controlled ZVS twin half-bridge high-frequency resonant inverter for induction heating," *IEEE Trans. Ind. Electron.*, vol.61, No.5, pp.2531–2545, May. 2014.

[26] J.Y. Lee and B.M. Han, "A bidirectional wireless power transfer EV charger using self-resonant PWM," *IEEE Trans. Power Electron.*, vol.30, No.4, pp.1784–1787, Apr. 2015.

[27] A. K. S. Bhat, "Analysis and design of LCL-type series resonant converter," *IEEE Trans. Ind. Electron.*, vol.41, No.1, pp.118–124, Feb. 1994.

[28] T. Mishima and M. Nakaoka, "A practical ZCS-PWM boost dc-dc converter with clamping diode-assisted active edge-resonant cell and its extended topologies," *IEEE Trans. on Ind. Electron.*, vol.60, no.6, pp.2225-2236, Jun. 2013.

[29] D.J. Thrimawithana, and U.K. Madawala, "A generalized steady-state model for bidirectional IPT systems," *IEEE Trans. Power Electron.*, vol.28, no.10, pp.4681-4689, Oct. 2013.

This article has been accepted for publication in a future issue of this journal, but has not been fully edited. Content may change prior to final publication. Citation information: DOI 10.1109/JESTPE.2019.2927723, IEEE Journal of Emerging and Selected Topics in Power Electronics

Tomokazu Mishima (S'00–M'04–SM'15) received the B.S., M.S., and Ph.D. degree all in electrical engineering from The University of Tokushima, Japan in 1999, 2001, and 2004 respectively. Since 2010, he has been with Kobe University, Hyogo, Japan as an associate professor, and engages in the researches and developments of power electronics circuits and systems. His research interests include soft-switching dc–dc converters, resonant converters, and high frequency inverters for industrial, automotive, renewable and sustainable energy applications.

Dr. Mishima is the recipient of the Best Paper Award in the Eighth IEEE International Conference on Power Electronics and Drive Systems (IEEE-PEDS 2009), Best Paper Presentation Award of the 2012 Annual Conference of the IEEE Industrial Electronics Society (IECON), and IEEE Transactions on Power Electronics 2017 Outstanding Reviewer Award. He serves as an associate editor of IEEE Transactions on Power Electronics and a secretary of IEEJ (The Institute of Electrical Engineering of Japan) Transactions on Industry Applications.

Dr. Mishima is a senior member of IEEJ, and a member of IEICE (The Institute of Electronics, Information and Communication Engineers), IEIEJ (The Institute of Electrical Installation of Japan), and JIPE (The Japan Institute of Power Electronics).